Solar Polarization 8
ASP Conference Series, Vol. 526
L. Belluzzi, R. Casini, M. Romoli, and J. Trujillo Bueno, eds.

On the Magnetic Nature of Solar Exploding Granules

S. L. Guglielmino,[1] V. Martínez Pillet,[2] B. Ruiz Cobo,[3,4] L. R. Bellot Rubio,[5] J. C. del Toro Iniesta,[5] S. K. Solanki,[6,7] and F. Zuccarello[1]

[1]*Dipartimento di Fisica e Astronomia "Ettore Majorana", Università degli Studi di Catania, Catania, Italy*
[2]*National Solar Observatory, Boulder, Colorado, USA*
[3]*Instituto de Astrofísica de Canarias, La Laguna, Tenerife, Spain*
[4]*Dep.to de Astrofísica, Univ. de La Laguna, La Laguna, Tenerife, Spain*
[5]*Instituto de Astrofísica de Andalucía, CSIC, Granada, Spain*
[6]*Max-Planck-Institut für Sonnensystemforschung, Göttingen, Germany*
[7]*School of Space Research, Kyung Hee University, Yongin, Gyeonggi-Do, Republic of Korea*

Abstract. We report on spectropolarimetric observations acquired by the imaging magnetograph SUNRISE/IMaX at high spatial (0.″3) and temporal (31.5 s) resolution during the first science flight of this balloon-borne solar observatory. We describe the photospheric evolution of an exploding granule observed in the quiet Sun. This granule is cospatial with a magnetic flux emergence event occurring at mesogranular scales (up to $\sim 12\,\mathrm{Mm}^2$ area). Using a modified version of the SIR code, we show that we can estimate the longitudinal field also in the presence of a residual cross-talk in these IMaX longitudinal measurements. We determine the magnetic flux content of the structure ($\sim 3\times10^{18}$ Mx), which appears to have a multipolar configuration, and discuss the origin of such flux emergence events.

1. Introduction

Exploding granules (EGs) appear as individual bright granules that expand by a larger amount than normal granular cells in the quiet Sun. Ultimately, after reaching a diameter of $4'' - 5''$ in about 10 minutes, they split into several smaller granules, representing the most intense case of fragmenting granules (Roudier et al. 2003). Since their first detection (Rosch 1960), several observational and numerical studies investigated EGs properties to explain this phenomenon (see Nordlund et al. 2009 for a review).

EGs are rather frequent, with a number density of about 4% (Mehltretter 1978), covering 2.5% of the observed photospheric area (Title et al. 1989). They share many observational characteristics with the family of large granules, i.e., granules with diameter larger than 1.″4 (Hirzberger et al. 1999a; Hirzberger 2002).

A central dark spot that hosts downflows of cool gas (Hirzberger et al. 1999b, 2001; Roudier et al. 2001; Berrilli et al. 2002) is usually observed in EGs. This feature appears to be linked to buoyancy braking (Massaguer & Zahn 1980).

The existence of EGs is connected to mesogranulation in hydrodynamical simulations (e.g., Simon et al. 1991). Actually, these structures are identified in observations with areas of positive divergence of the horizontal velocity (e.g., Roudier et al. 2003).

Although the morphological evolution of EGs is well known, their correlation with magnetic flux emergence events is not clear. Some observations found the presence of emerging flux in certain EGs (De Pontieu 2002; Socas-Navarro et al. 2004; Zhang et al. 2009; Palacios et al. 2012). This evidence has been related to the horizontal internetwork fields (HIFs) observed by Lites et al. (1996, 2008).

In this work, we analyze observations taken by the Imaging Magnetograph eXperiment (IMaX; Martínez Pillet et al. 2011) on board the Sunrise balloon-borne solar observatory (Solanki et al. 2010, 2017; Barthol et al. 2011). We follow the evolution of an EG at high spatial and temporal resolution. This feature is cospatial to a flux emergence episode that occurs at mesogranular scale and hosts patches with linear polarization signals. In the following, we describe the observations and the data analysis (Sect. 2), we report our results (Sect. 3), and we briefly draw our conclusions (Sect. 4).

2. Observations and Data Analysis

We analyzed spectropolarimetric IMaX data obtained on 2009 June 10, from 22:55:41 to 23:54:30 UT. During that time, IMaX acquired polarization maps every 31.5 s over a quiet Sun region at the disc center, covering a field of view (FOV) of $\sim 46'' \times 46''$. The spatial resolution of these observations is $0\farcs3$, with a pixel size of $0\farcs055$. Only the Stokes parameters I and V were measured (longitudinal observing mode), at twelve wavelength positions over the Fe I 525.02 nm line (Landé factor $g = 3$) every 3.5 pm from λ = -19.25 pm to λ = +19.25 pm with respect to the line center, with a spectral resolution of 8.5 pm. The FOV of these IMaX observations is displayed in Fig. 1.

Data reduction was performed using standard operations, i.e., dark-current removal and flat-field correction. The signal-to-noise ratio is about 1.2×10^{-3} in units of the continuum intensity per wavelength point for each Stokes parameter. In longitudinal observing modes, for which it is not possible to apply the demodulation matrix described by Martínez Pillet et al. (2011), a residual cross-talk in Stokes V is present in the reduced data. Pre-flight measurements provide an estimate of this cross-talk, that is

$$V_{\rm measured} = -0.88\, U_\odot + 0.55\, V_\odot \,, \tag{1}$$

where $U_\odot$ and $V_\odot$ refer to the *original* solar signals. To get rid of this issue, we carried out a non-standard inversion of the observed spectra by using a modified version of the SIR code (Ruiz Cobo & del Toro Iniesta 1992). First, we tested the reliability of these inversions by applying the modified code to IMaX data acquired in full spectropolarimetric mode (Guglielmino et al. 2012), inverting Stokes I and the linear combination (1). The results of this preliminary test confirmed that this version of the SIR code is able to extract information also from longitudinal spectropolarimetric measurements. We obtained a very good estimate of the longitudinal component of the magnetic field, $B_{\rm long}$, used to derive the magnetic flux density, and of the thermodynamical parameters (e.g., temperature, gaseous pressure).

The line-of-sight (LOS) velocity was derived from a Gaussian fit to the spectral points along the Stokes I profile, considering the Doppler shift of the line center. The instrumental blueshift was also removed. The velocity scale was calibrated by using a convective blueshift of ~ 200 m s^{-1} for the Fe I 525.02 nm line (Dravins et al. 1981).

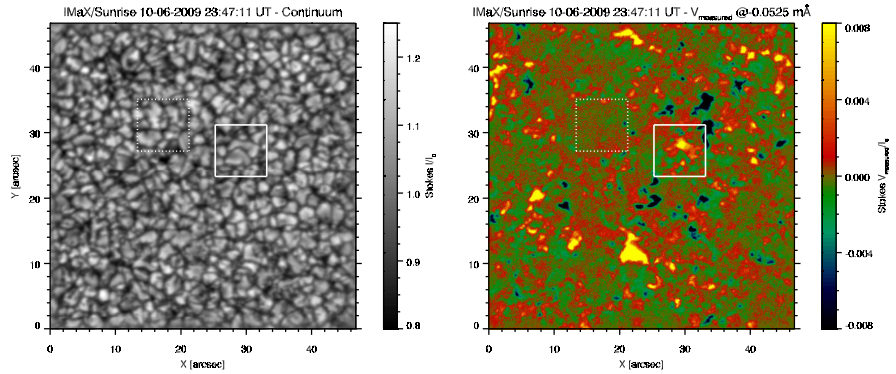

Figure 1. *Left panel*: Continuum intensity map. *Right panel*: $V_{\rm measured}$ signal map in the blue lobe of the measured Stokes *V*. The solid line box, which covers a subFOV of $\sim 8'' \times 8''$, indicates the location of the EG analyzed in this work. The dashed line box, with the same subFOV, indicates a region of very quiet Sun, used as a reference.

3. Results

Figure 2 illustrates the evolution of the EG. The first column displays the photospheric continuum, where we observe that this expanding structure forms a central dark spot (Δt = 252 s) and eventually splits into smaller granules (Δt = 504 s). The southernmost granule undergoes the same evolution (Δt = 768 s), until it splits into four granules.

The second column of Fig. 2 shows the integrated signal of $V_{\rm measured}$, given by

$$V_{\rm integrated} = \frac{1}{8\ \langle I_c \rangle} \sum_{i=1}^{8} \epsilon_i \, [V_{\rm measured}]_i \ , \qquad (2)$$

where $\langle I_c \rangle$ is the continuum intensity averaged over the IMaX FOV, i runs over the central eight wavelength positions, from λ = -12.25 pm to λ = +12.25 pm from the line center, and $\epsilon = [1, 1, 1, 1, -1, -1, -1, -1]$. The distribution of the magnetic areas, in particular of the neutral lines, can be derived from this quantity, because at first approximation it is null only in the regions where the magnetic field changes sign.

The EG is associated with an emerging flux region, as also pointed out by Palacios et al. (2012). A flux concentration with salt-pepper polarity appears at 23:36:42 UT, being located at [5″, 4″] in the subFOV shown in Fig. 2 (first row, second column). Magnetic field patches with opposite polarity appear close to each other. Notably, this occurs in the region where the first dark spot forms (Δt = 504 s), later becoming an intergranular lane (Δt = 768 s).

The LOS velocity, displayed in Fig. 2 (third column), indicates that the structure is generally characterized by upflows, except in the central dark dot where downflows are found (Δt = 504 s and Δt = 1008 s), in agreement with previous observations. Note that the LOS velocity may be affected by *p*-mode oscillations, that were not filtered.

The maps of magnetic flux density (Fig. 2, fourth columm) indicate that the distribution of the magnetic areas derived from $V_{\rm integrated}$ is representative of the real magnetic flux patches. Furthermore, they allow measuring the amount of emerged flux in the region of interest occupied by the EG, found to be about 3×10^{18} Mx.

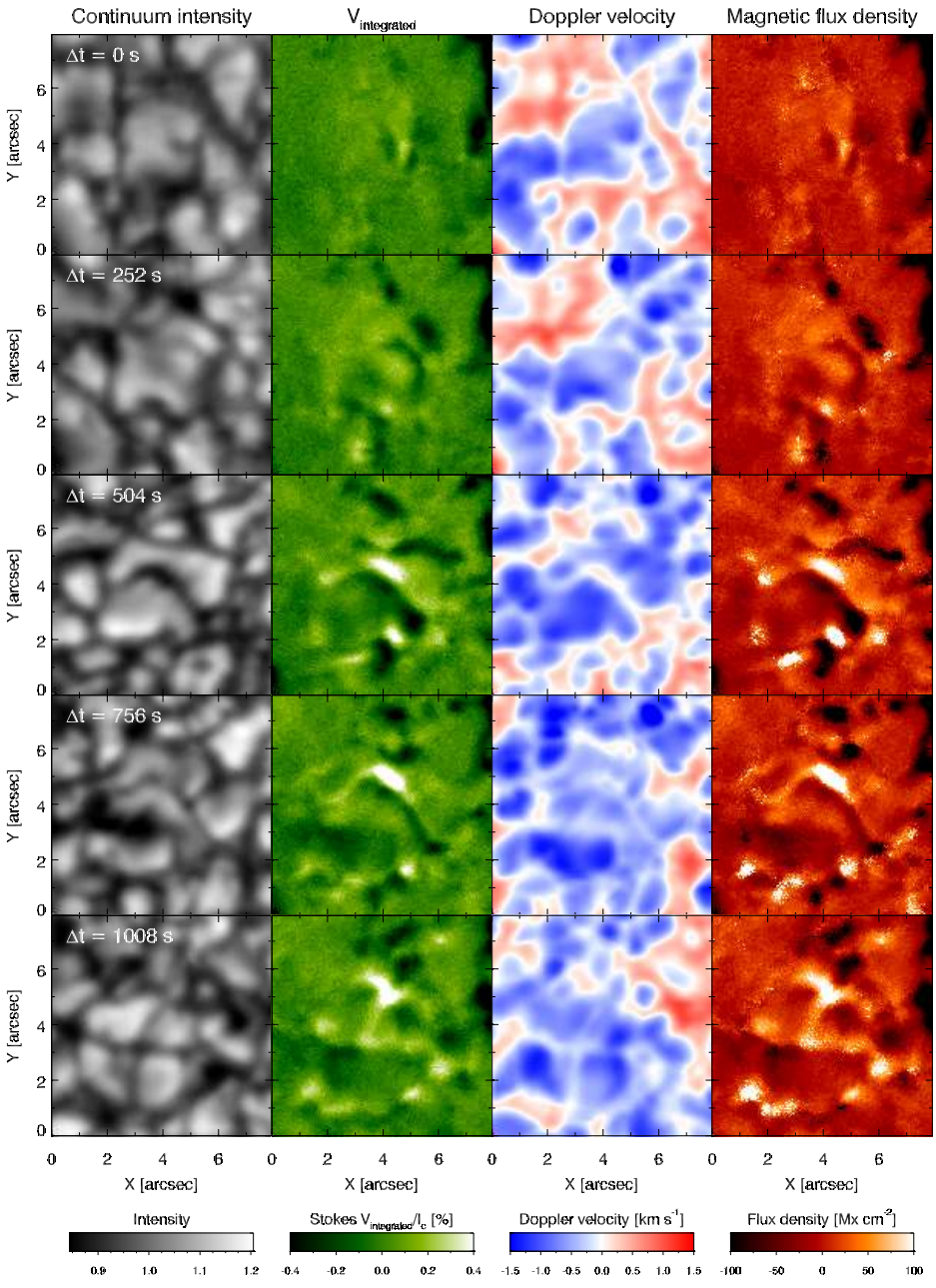

Figure 2. Time sequence showing the evolution of the EG, which appears to be cospatial to an emerging magnetic structure. The subFOV is indicated with a solid box in Fig. 1. Time runs from top to bottom, with a cadence of about 4 minutes.

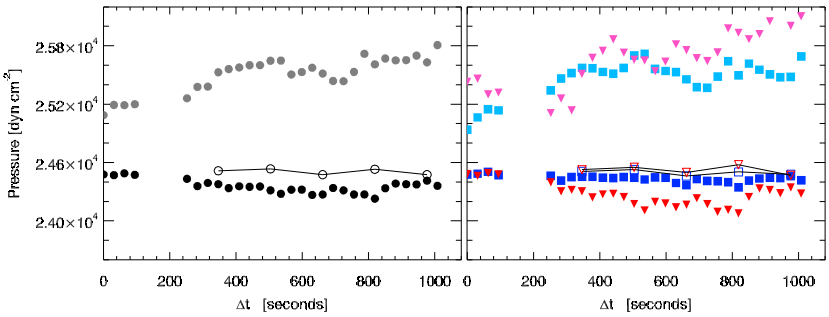

Figure 3. *Left panel*: Graph of the gaseous pressure (black circles) and of total pressure (grey circles) averaged within the box encompassing the EG (solid box in Fig. 1), and of the gaseous pressure (empty circles) averaged in the area occupied by a very quiet Sun region (dashed box in Fig. 1). *Right panel*: Same, for granular (squares, blue color scheme) and intergranular (triangles, red color scheme) regions, respectively, present in both subFOVs.

Figure 3 (left panel) shows the trend of the gaseous pressure averaged in the whole EG subFOV and in a very quiet Sun region, used for comparison. The total pressure (gaseous + magnetic) in the EG subFOV is also displayed. The plots suggests that magnetic pressure, due to the emerging field, appears to compensate the slight decrease of the gaseous pressure, required for magnetic buoyancy. By contrast, the pressure in very quiet Sun region exhibits a stationary trend pattern.

Figure 3 (right panel) shows the same quantities, for granules and intergranular lanes separately. For this purpose, we applied a discrimination based on the continuum brightness of these features. Points brighter/darker than their surroundings by at least 3% (rms contrast of the granulation) are taken to be granules/intergranular lanes. Both granular and intergranular regions are affected by the presence of the magnetic field, even if the effect on intergranules is slightly more pronounced.

4. Conclusions

The overall characteristics suggest that we observe an emerging multi-polar magnetic flux mantle structure, which is able to disturb the granulation pattern. The detection of this feature is favoured by the high polarimetric sensitivity of IMaX.

Numerical simulations predict that, at the site of flux emergence, the additional magnetic pressure is able to sustain the horizontal expansion velocity of the granules, giving rise to abnormal granulation. The origin of such flux-mantle magnetic structures may reside in weakly twisted magnetic fields, which are fragmented on their way to the photosphere as coherent flux bundles, or may be the result of a local dynamo process in the near-surface layers, which generates horizontal structures in the quiet Sun. Further investigations on the properties of these structures are required to find an answer.

Acknowledgments. This research work has received funding from the European Commission's Seventh Framework Programme under the grant agreements no. 312495 (SOLARNET project). This research is also supported by the ITA MIUR-PRIN 2012 grant on "The active sun and its effects on space and Earth climate" and by Space Weather Italian COmmunity (SWICO) Research Program.

References

Barthol, P., Gandorfer, A., Solanki, S. K., et al. 2011, Solar Phys., 268, 1
Berrilli, F., Consolini, G., Pietropaolo, E., et al. 2002, A&A, 381, 253
De Pontieu, B. 2002, ApJ, 569, 474
Dravins, D., Lindegren, L., & Nordlund, A. 1981, A&A, 96, 345
Guglielmino, S. L., Martínez Pillet, V., Bonet, J. A., et al. 2012, ApJ, 745, A160
Hirzberger, J. 2002, A&A, 392, 1105
Hirzberger, J., Bonet, J. A., Vázquez, M., & Hanslmeier, A. 1999a, ApJ, 515, 441
—. 1999b, ApJ, 527, 405
Hirzberger, J., Koschinsky, M., Kneer, F., & Ritter, C. 2001, A&A, 367, 1011
Lites, B. W., Kubo, M., Socas-Navarro, H., et al. 2008, ApJ, 672, 1237
Lites, B. W., Leka, K. D., Skumanich, A., et al. 1996, ApJ, 460, 1019
Martínez Pillet, V., Del Toro Iniesta, J. C., Álvarez-Herrero, A., et al. 2011, Solar Phys., 268, 57
Massaguer, J. M., & Zahn, J.-P. 1980, A&A, 87, 315
Mehltretter, J. P. 1978, A&A, 62, 311
Nordlund, Å., Stein, R. F., & Asplund, M. 2009, Living Rev.Sol.Phys., 6, 2
Palacios, J., Blanco Rodríguez, J., Vargas Domínguez, S., et al. 2012, A&A, 537, A21
Rosch, J. 1960, in IAU Symp. 12, Aerodynamic Phenomena in Stellar Atmospheres, ed. R. N. Thomas (Bologna: Zanichelli), 313
Roudier, T., Eibe, M. T., Malherbe, J. M., et al. 2001, A&A, 368, 652
Roudier, T., Lignières, F., Rieutord, M., et al. 2003, A&A, 409, 299
Ruiz Cobo, B., & del Toro Iniesta, J. C. 1992, ApJ, 398, 375
Simon, G. W., Title, A. M., & Weiss, N. O. 1991, ApJ, 375, 775
Socas-Navarro, H., Martínez Pillet, V., & Lites, B. W. 2004, ApJ, 611, 1139
Solanki, S. K., Barthol, P., Danilovic, S., et al. 2010, ApJ, 723, L127
Solanki, S. K., Riethmüller, T. L., Barthol, P., et al. 2017, ApJS, 229, 2
Title, A. M., Tarbell, T. D., Topka, K. P., et al. 1989, ApJ, 336, 475
Zhang, J., Yang, S.-H., & Jin, C.-L. 2009, Res.Astron.Astrophys., 9, 921